An analytical frequency-domain model of self-sensing magnetic bearing: modulation approach

Jie YU, Changsheng ZHU
College of Electrical Engineering, Zhejiang University
38# Zheda road, Hangzhou, China
E-mail: yujie.zjuee@hotmail.com

Abstract

This article introduces an analytical model of the self-sensing process in the self-sensing active magnetic bearings. In this model, the switching harmonics of the PWM amplifier and the demodulator's output are expressed analytically in the frequency domain, thus the nonlinear self-sensing process can be regarded as a "virtual displacement sensor" with precise input-output relationships. Then, the sensitivity of the virtual displacement sensor is investigated, which indicates that the virtual sensor's sensitivity not only has varying values with different system parameters but also deteriorates significantly in the high frequency region. Fortunately, an acceptable sensitivity of the virtual displacement sensor can still be maintained if the system is properly designed, which is also verified by experimental results on a four degree-of-freedom self-sensing radial AMBs rigid rotor platform.

Keywords : Self sensing active magnetic bearing, Modulation approach, Analytical model, Virtual displacement sensor, Sensitivity

1. Introduction

The Self-Sensing Active Magnetic Bearing (SSAMB) technology has been intensively researched in the past few decades for its advantages in system integration, cost and installation. While the Linear Time Invariant (LTI) state observer is utilized to realize the SSAMB (Vischer and Bleuler, 1993) at the very beginning, the high frequency interrogation signal based techniques have become the research hotspots in the past years (Maslen, 2006). Except the interrogation signal injection method (Park et al., 2008), the switching harmonics of the Pulse Width Modulation (PWM) power amplifier can be conveniently utilized as the interrogation signal to realize the SSAMBs.

Noh (1996) introduced a close loop parameter estimator, in which an induction model of the magnetic pole is embedded, for rotor displacement estimation. The accuracy of embedded model and the close loop estimator's stability are vital for the self-sensing performance. Schammass, et al. (2005) proposed an open loop self-sensing method, in which the estimation error caused by duty cycle variation and magnetic saturation are both compensated. For these two approaches, amplitude demodulators are necessary to extract and obtain the amplitude variation of the fundamental component of the switching harmonics.

To reduce the phase lag caused by filters of the demodulator and fully utilize higher order components of the switching harmonics, the current slope of the coil current can be directly measured and applied for self-sensing (van Schoor et al., 2013). However, the nonlinear eddy current effect becomes a big challenge for precisely measuring the current slope (Wang and Binder, 2014). In addition, experimental results show that the direct current slope measurement method is also sensitive to duty cycle variations in practice (Richter et al., 2014).

Although the linear periodic model have been proposed for robustness analysis of these interrogation signal based SSAMBs (Maslen et al., 2006), it's actually obscure for practical applications. In this paper, we want to model the "modulation approach" SSAMB, in which demodulators and the open loop self-sensing method are used, in a more practical way. Firstly, the switching harmonics of the two-state PWM power amplifier are modeled in the frequency domain, and the analytical expression of the demodulator's output is obtained. Then, we regard the self-sensing process as a "virtual displacement sensor" and investigate how its sensitivity value varies with different system parameter and

under different control current. Finally, to validate the theoretical analyses, step response and rotor rotation experiment are implemented on a four Degree of Freedom (DOF) radial SSAMBs rigid rotor platform,

2. The analytical model of the self-sensing process in SSAMB

The nonlinear techniques used for self-sensing make it difficult to model and analyze the SSAMB system. For the modulation-approach SSAMB, these nonlinear techniques include the switching power amplifier and the demodulator. In this paper, the current mode two-state PWM power amplifier and the commonly used demodulator, consisting of a bandpass filter and an envelope detector, are employed. And the AMB is particular the eight-pole heteropolar radial active magnetic bearing, thus it's unnecessary to consider the cross-coupling between adjacent magnetic poles.

2.1 The model of switching harmonics of the switching power amplifier

When the coil of AMB is driven by the PWM power amplifier, there exist high frequency switching ripples in the coil current. The switching ripples consists of numerous switching harmonic components. For AMB with sensors, these switching harmonics are neglected, so that the switching power amplifier can be modeled as a first order inertial element. But for the modulation-approach SSAMB, the fundamental component of switching harmonics in coil current is utilized to realize the self-sensing process.

Figure 1 illustrates the switching ripples of the output voltage $V(t)$ and current $i(t)$ of the two-state switching power amplifier, in which V_s is the bus voltage, T_s is the switching period and α is the PWM duty cycle in the k-th switching period.

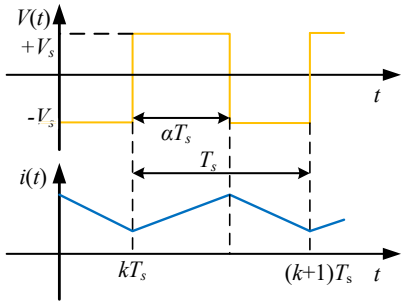

Fig. 1 the switching ripple in the output of the switching power amplifier

If the turn-on and turn-off time of the switching components in power amplifier are ignored, the output voltage $V(t)$ of the two-state PWM power amplifier can be modeled as PWM square waveform,

$$V(t)=\begin{cases}V_s & kT_s<t\le kT_s+\alpha T_s\\ -V_s & (k+\alpha)T_s<t\le(k+1)T_s\end{cases} \tag{1}$$

Within the k-th switching period, $V(t)$ can be expanded into Fourier series as,

$$V(t)=(2\alpha-1)V_s+\sum_{n=1}^{\infty}\frac{4V_s}{n\pi}\left|\sin(n\pi\alpha)\right|\cos(n\omega_s t+\varphi_n) \tag{2}$$

where $\omega_s=2\pi/T_s$ is the switching angular frequency, $\varphi_n=-n\pi\alpha$ is the phase angle of the n-th order harmonic. In Eq. (2), the $(2\alpha\text{-}1)V_s$ item relates to the expected output tracking the power amplifier's reference input, and the sum item corresponds to high frequency switching harmonics.

The PWM duty cycle α is mainly determined by the reference input of power amplifier, $i_{ref}(t)$. As an example, we set $i_{ref}(t)=I_0+I_c\cos(2\pi f_c t)$, in which I_0 is the bias current, I_c and f_c are respectively the amplitude and frequency of the control current. And the Kirchhoff's law is utilized for the coil load circuit driven by the power amplifier,

$$v_{ref}(t)=L\frac{\mathrm{d}i_{ref}(t)}{\mathrm{d}t}+i_{ref}(t)R=I_0R+I_c\sqrt{R^2+(\omega_c L)^2}\cos(2\pi f_c t+\theta) \tag{3}$$

where L is the coil inductance, $\omega_c=2\pi f_c$ is the angular frequency of the control current and $\theta=\arctan(R/\omega_c L)$ is the impedance angle of the coil load.

Referring to Eq. (2), the relationship below holds,

$$v_{ref}(t)=V_s(2\alpha-1) \tag{4}$$

Then the PWM duty cycle of power amplifier can be calculated as,

$$\alpha=0.5+\frac{I_0R}{2V_s}+\frac{I_c\sqrt{R^2+(\omega_cL)^2}}{2V_s}\cos(2\pi f_ct+\theta),\ \alpha\in[0,1] \tag{5}$$

In high frequency region, the coil's inductive impedance $jn\omega_sL$ is much larger than the coil resistance R so that the effect of R can be neglected. According to the superposition principle, the fundamental component of switching harmonics in coil current can be expressed as,

$$i_1(t)=\frac{4V_s}{\pi\omega_sL}\sin(\pi\alpha)\sin(\omega_st-\pi\alpha) \tag{6}$$

For the coil inductance L, if the magnetic saturation of ferromagnetic iron core is avoided, L is inversely proportional with the rotor air gap x,

$$L=\frac{\mu_0N^2A_g}{2x} \tag{7}$$

where μ_0 is the magnetic permeability of free space, N is the number of turns of coil and A_g is the cross-sectional area of the flux path at the air gap.

Combining Eqs. (6) and (7), $i_1(t)$ can be further expressed as,

$$i_1(t)=\frac{8V_sx}{\pi\omega_s\mu_0N^2A_g}\sin(\pi\alpha)\sin(\omega_st-\pi\alpha) \tag{8}$$

Eq. (8) shows that the amplitude of $i_1(t)$ is a function of both rotor air gap x and PWM duty cycle α, and the phase of $i_1(t)$ is also affected by α. Therefore, in the signal processing perspective, $i_1(t)$ is a mixed signal modulated in both amplitude and phase.

2.2 The analytical expression of the demodulator's output

For the modulation-approach SSAMB, the demodulator is essential to extract and demodulate $i_1(t)$ from coil current $i(t)$. Fig. 2 gives a typical amplitude demodulator diagram to process the modulated signal $i_1(t)$. The bandpass filter extracts $i_1(t)$ from the measured signal of coil current $i(t)$. The envelope detector, which consists of an Absolute (ABS) value function circuit and a lowpass filter, demodulates the amplitude information of $i_1(t)$ as $|i(t)|_{LF}$.

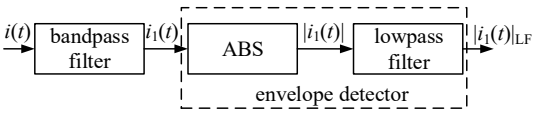

Fig. 2 The diagram of the demodulator for self-sensing

Because the ABS part of the demodulator is nonlinear, it is difficult to precisely model how $i_1(t)$ is processed within the envelope detector. But by utilizing the Fourier cosine series of the absolute value function,

$$|u|=\frac{\pi}{2}-\frac{4}{\pi}\sum_{n=0}^{\infty}\frac{\cos[(2n+1)u]}{(2n+1)^2} \tag{9}$$

it is possible to model the self-sensing process in the demodulator in frequency domain and get an analytical expression of the demodulator's output.

Combining Eq. (8) and Eq. (17), the output of ABS can be expressed as,

$$\left|i_1(t)\right| = \frac{\pi}{2} - \frac{4}{\pi}\sum_{n=0}^{\infty}\frac{\cos\left[(2n+1)G_{\mathrm{BPF}}i_1(t)\right]}{(2n+1)^2} \tag{10}$$

where G_{BPF} is the passband gain of the bandpass filter.

By defining variables z_1 and z_2,

$$\begin{aligned} z_1 &= \frac{4V_s(2n+1)G_{BPF}x}{\pi\omega_s\mu_0N^2A_g}\sin(2\pi\alpha) \\ z_2 &= \frac{4V_s(2n+1)G_{BPF}x}{\pi\omega_s\mu_0N^2A_g}(1-\cos(2\pi\alpha)) \end{aligned} \tag{11}$$

and utilizing trigonometric identities and Jacobi-Anger identities of,

$$\begin{aligned} \sin(z\sin\varphi) &= 2\sum_{v=1}^{\infty}J_{2v-1}(z)\sin((2v-1)\varphi) \\ \cos(z\sin\varphi) &= J_0(z) + 2\sum_{v=1}^{\infty}J_{2v}(z)\cos(2v\varphi) \end{aligned} \tag{12}$$

the frequency spectrum of $|i_1(t)|$ can be analytically divided into low frequency components with $\omega<\omega_s$ and high frequency components with $\omega\geq\omega_s$.

$$\left|i_1(t)\right| = \left|i_1(t)\right|_{\mathrm{LF}} + \left|i_1(t)\right|_{\mathrm{HFC}} + \left|i_1(t)\right|_{\mathrm{HFS}} \tag{13}$$

in which $|i_1(t)|_{\mathrm{LF}}$ consists of low frequency components of $|i_1(t)|$, $|i_1(t)|_{\mathrm{HFC}}$ consists of the central frequency components of the $2v\omega_s$ frequency bands, and $|i_1(t)|_{\mathrm{HFS}}$ consists of the sideband frequency components of the $2v\omega_s$ frequency bands. The analytical expression of $|i_1(t)|_{\mathrm{LF}}$ is,

$$\left|i_1(t)\right|_{\mathrm{LF}} = \frac{\pi}{2} - \sum_{n=0}^{\infty}\frac{4}{(2n+1)^2\pi}\left[J_0(z_1)J_0(z_2) + 2\sum_{v=1}^{\infty}(-1)^v J_{2v}(z_1)J_{2v}(z_2)\right] \tag{14}$$

If the high frequency components are fully attenuated by the lowpass filter of demodulator, $|i_1(t)|_{\mathrm{LF}}$ is just the demodulator's output.

3. The sensitivity of the "virtual displacement sensor" of SSAMB

The main difference between AMB with sensors and SSAMB is how the rotor displacement is measured. For the former, individual displacement sensors are utilized, whose sensor sensitivity is constant. In other words, a certain rotor displacement always result in the same value change in the sensor's output, regardless of the operation status and parameters variations of the AMB. While for the latter, it's much more complicated. Since the analytical expression of the demodulator's output has been obtained in section 2, we can regard the self-sensing process of SSAMB as a "virtual displacement sensor", and define the sensitivity S of the virtual displacement sensor as the normalized ratio between the demodulator's output and the real rotor displacement.

$$S \triangleq \frac{\partial\left|i_1(t)\right|_{\mathrm{LF}} / \left|i_1(t)\right|_{\mathrm{LF0}}}{\partial x / x_0} \tag{15}$$

where $|i_1(t)|_{\mathrm{LF0}}$ is the demodulator's output when rotor is kept still with the nominal air gap x_0 and the coil is only driven by the bias current I_0.

It is obvious that a high and stable sensitivity value is preferred for the SSAMB. But as Eq. (14) shows, the demodulator's output is both affected by control current and parameter values of the SSAMB. To investigate the property of the virtual displacement sensor's sensitivity, we change the value of one parameter around its nominal one each time, and keep the other parameters with their nominal values. These changed parameters includes the passband gain of the bandpass filter of demodulator G_{BPF}, the coil inductance at the nominal air gap L_0, the coil resistance R, the bus voltage of the power amplifier V_s and the switching frequency of the power amplifier f_s. The nominal values of SSAMB's parameters are listed in Tab. 1.

Tab. 1 Nominal parameter values of the SSAMB

Variable	Symbol/ Unit	Value
Nominal air gap	x_0 /mm	0.35
Coil resistance	R /Ω	1.5
Nominal coil inductance	L_0 /mH	7
Bias current	I_0 /A	1.2
Bus voltage of power amplifier	V_s /V	50
Switching frequency of power amplifier	f_s /kHz	15
Passband gain of bandpass filter	G_{BPF} /dB	18.2

To simulate different operation statuses of the SSAMB, the frequency of the control current is set as f_c=100Hz, 300Hz, 500Hz, 700Hz and 900Hz, respectively, and the amplitude of the control current is set as $I_c=I_0$. Fig.3 plots the sensitivity of the virtual displacement sensor with different parameter values and under different control current.

As Fig. 3(a), 3(c) and 3(e) show, when f_c≤700Hz, the sensitivity S, though decreases slowly as f_c increases, is not obviously affected by the variation of G_{BPF}, R and f_s. But when f_c>700Hz, a significant deterioration of S occurs. In the latter case, the increase of G_{BPF}, the decrease of R and f_s all contribute to a higher S value.

As Fig. 3(b) and 3(d) show, when f_c>100Hz, the increase of L_0 and the decrease of V_s both lead to a worse S value as f_c increases. And if the bandwidth limit of the power amplifier is reached, the worst S values are achieved.

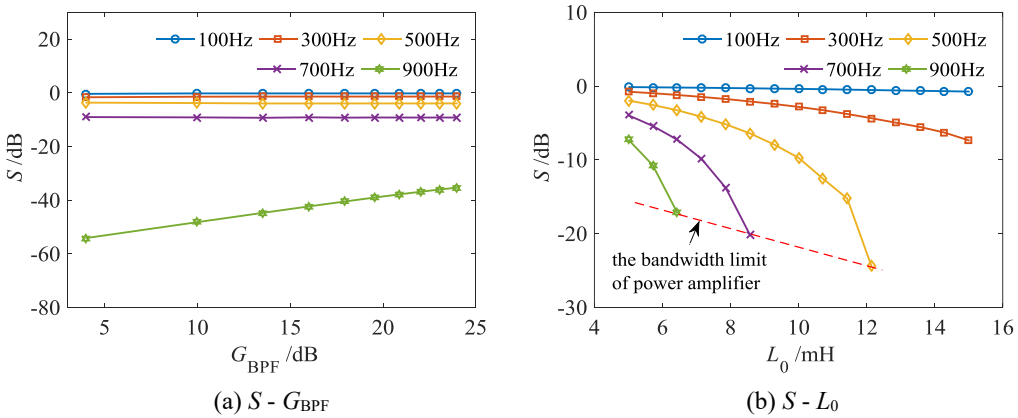

(a) S - G_{BPF} (b) S - L_0

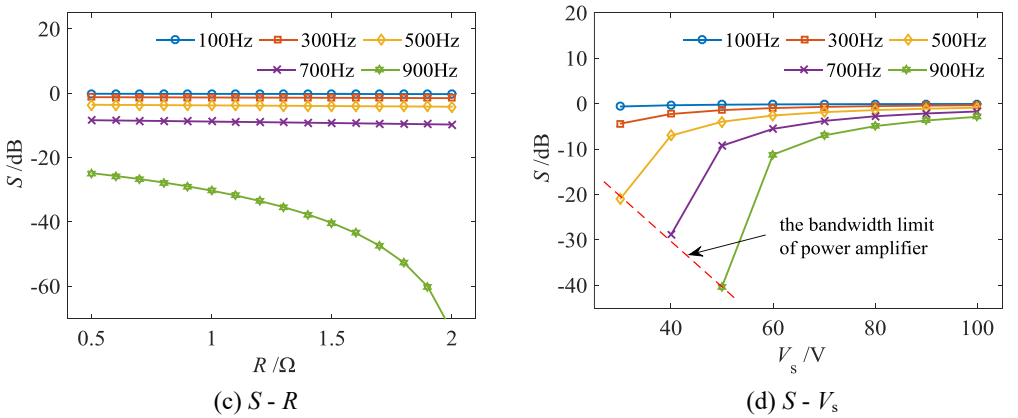

(c) S - R (d) S - V_s

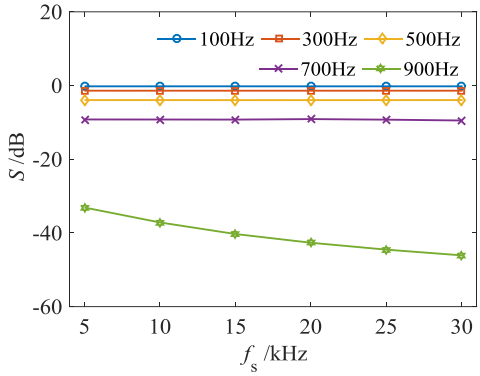

(e) S - f_s

Fig. 3 The sensitivity of the "virtual displacement sensor"

Although numerous duty cycle compensation methods can be utilized to reduce the effect of duty cycle on the demodulator's output, the varying sensitivity property of the virtual displacement sensor may still result in poor self-sensing accuracy of the SSAMB, especially when f_c is high. But if the SSAMB is properly designed so that an acceptable sensitivity of the virtual displacement sensor is maintained, the performance of the SSAMB can still be guaranteed.

4. Experiment results

A four-DOF radial SSAMBs rigid rotor platform is utilized for self-sensing suspension experiment. In the platform, the radial AMBs are eight-pole heteropolar magnetic bearings, the power amplifier is the current mode two-state PWM power amplifier and the analog demodulator consists of an 8th order bandpass filter, an absolute value function circuit and a 3th order lowpass filter (CRC π-filter). A TMS320F28335 DSP board is applied for calculation and control. The photo of the experimental platform is shown in Fig. 4.

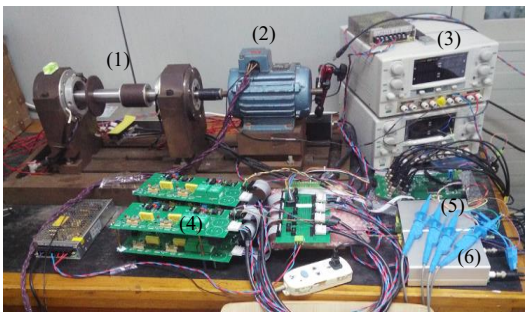

Fig. 4 The experimental platform. (1) radial SSAMBs and rigid rotor. (2) Induction motor.
(3) Power supply. (4) Power amplifier. (5) DSP control board. (6) Analog demodulator board

With important parameters selected according to the analyses in section 3, main parameters of the experimental platform are listed in Tab. 2.

In the experiment, the duty-cycle compensated demodulator's output $|i_1(t)|_{LFc}=|i_1(t)|_{LF}/\sin(\pi\alpha)$ is utilized as the feedback signal of the SSAMB system, and the PID controller is applied for rotor position control. With four-DOF self-sensing suspension of rotor, the step response and rotor rotation experiment of the SSAMB are implemented.

Figure 5 shows the estimated and measured rotor displacement on the y-axis when a constant disturbance force is added on the rotor middle in the vertical direction at time 0.7s, and removed at time 1s. There are no evident error and delay between the estimated and measured rotor displacement, which means a good self-sensing performance. Fig. 6 shows the rotor locus when the rotor is rotating at 3000rpm, in which the amplitude of rotor vibrations is smaller than 0.1mm.

The experimental results above indicate good robustness and dynamic performance of SSAMB, which also validate

the feasibility of system parameters that are selected according analyses in section 3.

Tab. 2 Main parameters of the experimental platform

Variable	Symbol/ Unit	Value
Rotor mass	m /kg	3.31
Rotor length	l /m	0.34
Nominal air gap	g_0 /mm	0.35
Coil resistance	R /Ω	1.5
Nominal coil inductance	L_0 /mH	7
Bias current	I_0 /A	1.2
Bus voltage of power amplifier	V_s /V	70
Switching frequency of power amplifier	f_s /kHz	15
Passband gain of bandpass filter	G_{BPF} /dB	18.2
passband of band pass filter	f_{BPF}/kHz	[13.52, 17.63]
cut off frequency of lowpass filter	f_{LPF}/kHz	1.6

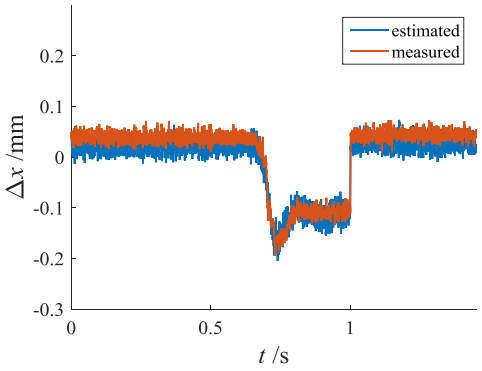

Fig. 5 step response of the SSAMB

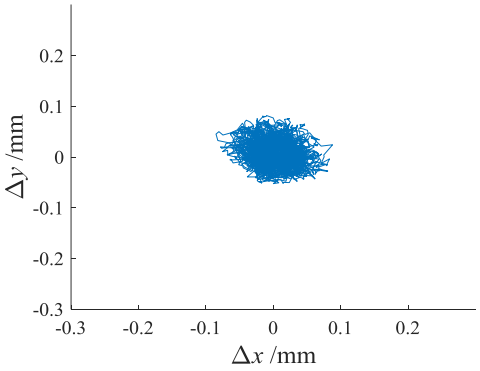

Fig. 6 rotor locus at rotation speed 3000rpm

5. Conclusions

Comparing with the AMBs with individual displacement sensors, the self-sensing process in the SSAMBs can be regarded as a virtual displacement sensor. Being different from the individual displacement sensor, the sensitivity value of the virtual sensor in the modulation-approach SSAMB is is variable under different system parameters and system operation status. The poor sensitivity of the virtual sensor deteriorates the self-sensing performance of SSAMB, even if compensation methods, whose accuracy is actually limited, are implemented. And this phenomenon is much more evident in the high frequency region. Fortunately, if system parameters are properly selected so that acceptable sensitivity of the virtual sensor is maintained, a satisfying system robustness and dynamic performance can still be achieved.

Acknowledgement

This work was sponsored by National Natural Science Foundation of China (51477155、11172261), Natural Science Foundation Project of Zhejiang Province (LZ13E070001), and Project of Collaborative Innovation Center of Advanced Aero-engine.

References

Maslen, E. H., Montie, D. T. and Iwasaki. T., Robustness limitations in self-sensing magnetic bearings, Journal of Dynamic Systems, Measurement and Control, Vol.128, No.2 (2006), pp.197–203.

Maslen, E. H., Self-sensing for active magnetic bearings: overview and status, Proceedings of the 10th International Symposium on Magnetic Bearings (2006), pp.13–19.

Richter, M., Schaede, H. and Rinderknecht, S., Investigations on the "direct digital inductance estimation"-concept for self-sensing AMBs under influence of eddy currents, Proceedings of the 14th International Symposium on Magnetic Bearings (2014), pp.693-698.

Noh, M. D., Self-sensing magnetic bearing driven by a switching power amplifier (1996). PhD Thesis, School of Engineering and Applied Science, University of Virginia.

Park, Y. H., Han, D. C. and Park, I. H. et al., A self-sensing technology of active magnetic bearings using a phase modulation algorithm based on a high frequency voltage injection method, Journal of Mechanical Science and Technology, Vol.22, No.9 (2008), pp.1757–1764.

Schammass, A., Herzog, R., Buhler, P. and Bleuler, H., New results for self-sensing active magnetic bearings using modulation approach, IEEE Transactions on Control Systems Technology, Vol.13, No.4 (2005), pp.509–516.

van Schoor, G., Niemann, A. C. and du Rand, C. P., Evaluation of demodulation algorithms for robust self-sensing active magnetic bearings, Sensors and Actuators A: Physical, Vol.189, No.1 (2013), pp.441–450.

Vischer, D. and Bleuler, H., Self-sensing active magnetic levitation, IEEE Transactions on Magnetics, Vol.29, No.2 (1993), pp.1276–1281.

Wang, J. and Binder, A., Position estimation for self-Sensing magnetic bearings based on double detection of current slopes, Proceedings of the 14th International Symposium on Magnetic Bearings (2014), pp.673–678.